

Tailoring Underwater Laser Acoustic Pulses

T.G. Jones,¹ M. Helle,¹ A. Ting,¹ and M. Nicholas²

¹Plasma Physics Division

²Acoustics Division

Introduction: The Naval Research Laboratory is developing a novel Remote Underwater Laser Acoustic Source (RULAS) to enable an airborne laser to remotely generate underwater acoustic pulses. Our acoustic source uses patented¹ optical compression techniques that produce underwater plasmas, heat them, and create intense acoustic pulses, all without the need for any hardware in the water. We primarily use Nd:YAG lasers with few-nanosecond pulse duration and a wavelength of 532 nm, which propagates readily through water. Our recent developments enable users to control both the duration and directivity of the acoustic pulses, in real time, by varying basic laser pulse parameters. The RULAS acoustic source is the first of its kind to allow such control, and accordingly it offers numerous potential new applications. In a milestone demonstration, we also conducted the first open water laser acoustic generation and propagation experiments, showing that RULAS techniques work in field conditions as well as in the lab.

Compact, high-repetition-rate lasers with appropriate pulse energy are commercially available and could be steered with rapidly movable mirrors from an airborne platform. Such a setup would be useful for several Navy and commercial applications, including

remote aircraft communications with undersea vessels and equipment such as unmanned underwater vehicles (UUVs), as well as for undersea navigation via remotely generated acoustic beacons. RULAS could also be combined with conventional or advanced opto-acoustic sensors to enable rapid sonar search and detection of underwater mines and vessels, as well as mapping of underwater terrain.

Acoustic Pulse Control Demonstrated: The propagation of acoustic pulses depends on the overall distribution of their component frequencies, in particular the frequency with the highest power within that distribution, denoted f_{peak} . Since the attenuation of a propagating acoustic pulse is proportional to the square of f_{peak} , f_{peak} determines the pulse's range, with lower f_{peak} corresponding to a longer range. Important intermediate acoustic range (greater than 100 m) applications require relatively long duration acoustic pulses, and corresponding low f_{peak} values. We recently developed ways to reduce f_{peak} by more than an order of magnitude compared to previous experiments, from 200 kHz to 15 kHz. The potential range of a laser-generated signal is thereby increased more than tenfold. In addition, we have learned how to control the acoustic source directivity. We have demonstrated sources with uniform intensity in all directions, or with a 20 dB variation between the direction of the laser beam and angles perpendicular to it, or with intermediate directivity variations.

Underwater plasma imaging in our lab experiments revealed that f_{peak} depends on the volume and

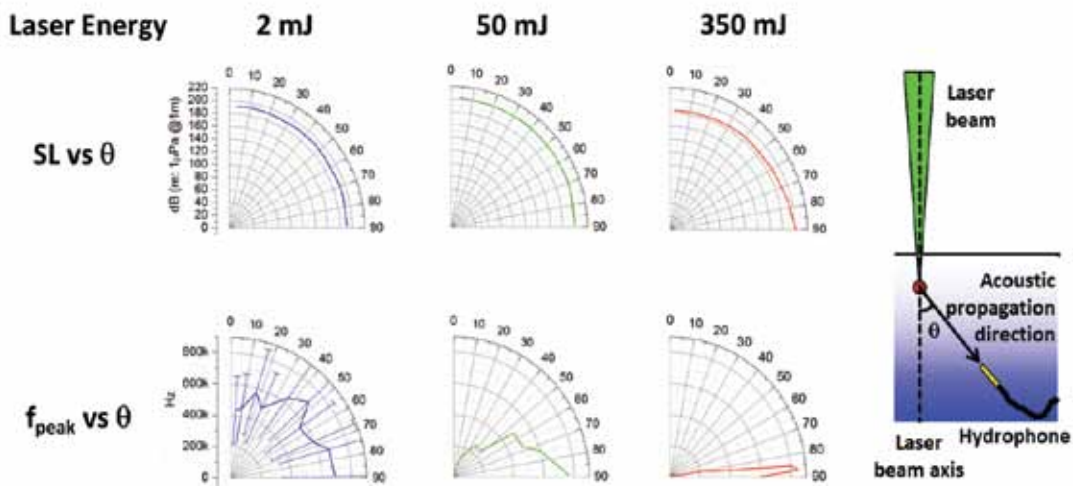


FIGURE 1

Plots of the acoustic source directivity (peak acoustic pressure, SL, vs acoustic propagation direction, θ) are shown in the top row for three different laser pulse energies. Plots of the peak frequency of the acoustic power spectrum dependence on acoustic propagation direction (f_{peak} vs θ) are shown in the bottom row for the same three laser energies. These plots illustrate the flexibility of this acoustic source, for which the acoustic pulse duration and radiation pattern can be quickly varied by adjusting basic laser parameters such as pulse energy.

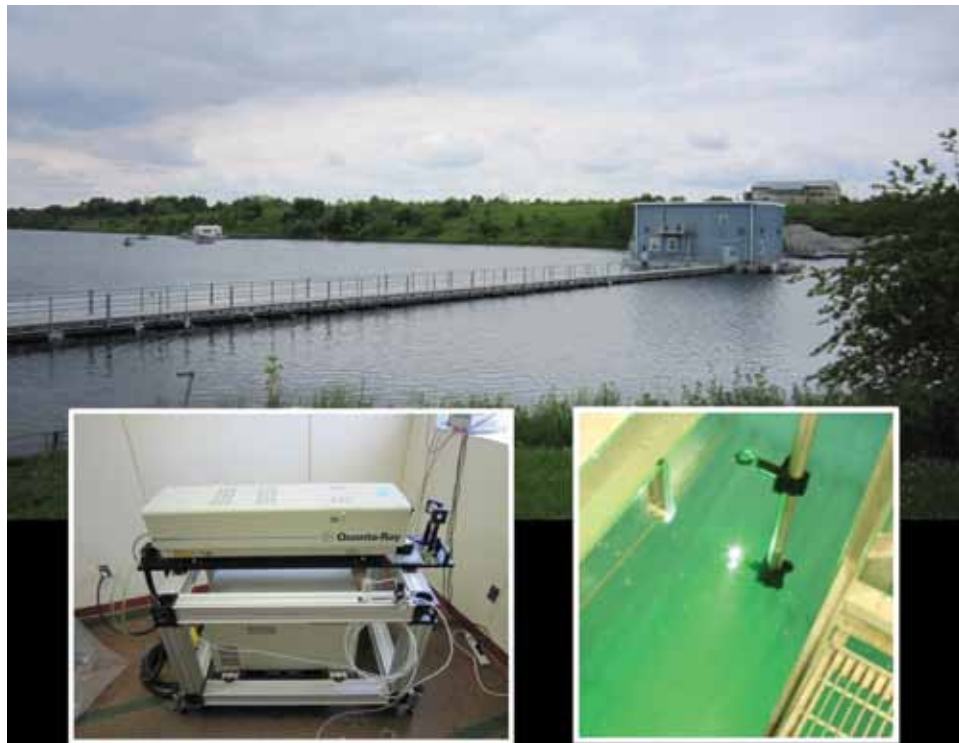


FIGURE 2
 In recent field experiments, laser pulses from a Nd:YAG laser (bottom left) housed in a floating structure (top, at right) were focused into the water (bottom right), generating underwater acoustic pulses. Acoustic pulse propagation was measured by hydrophones on a distant boat (top, at left).

shape of the underwater plasma. Most important, we found that we can control the plasma volume and shape by varying basic laser parameters including pulse energy, focusing angle, and laser intensity at the water surface. For nanosecond laser pulses, larger energy and shallower focusing angles produce more elongated plasmas. We generated a variety of plasma shapes from near-spherical, with dimension of a few millimeters, to an elongated cylindrical shape, with length of up to 5 cm. These different plasma shapes resulted in acoustic pulses with dramatically different directivity and frequency content, as illustrated in Fig. 1.

First Open Water Demonstration: Another recent accomplishment was our first open water demonstration of RULAS laser acoustic generation and acoustic propagation. We performed these tests in 2010 and 2011 at the Lake Glendora Test Facility of Naval Surface Warfare Center, Crane Division, using a laser in a floating platform on the lake, as shown in Fig. 2. Steering mirrors and a lens focused the laser pulses into the water, with each pulse generating an acoustic source level of about 190 dB (referenced to 1 micropascal at 1 m from the source). Acoustic pulse propagation was measured by boat-mounted hydrophones at distances up to 300 m (approximately 1000 ft). Prior laboratory

acoustic propagation distances were limited to about 3 m. These field experiments verified that there was no significant ultrasonic attenuation during acoustic propagation at these ranges, and included the first intermediate distance acoustic directivity measurements of the RULAS source.

Summary: Recent development of the Remote Underwater Laser Acoustic Source technology yielded an order of magnitude improvement in acoustic source level (to 235 dB), an order of magnitude reduction in peak acoustic frequency (to 15 kHz), and more than an order of magnitude increase in acoustic range. In addition, a successful first demonstration of RULAS laser acoustic generation and acoustic propagation in an open water environment was performed. These improvements greatly increased the utility and flexibility of this novel acoustic source, and open water field tests demonstrated its potential for a wide variety of applications.

[Sponsored by the NRL Base Program (CNR funded)]

Reference

¹T.G. Jones, A.C. Ting, P.A. Sprangle, L.D. Bibee, and J.R. Peñano, "Remote Underwater Laser Acoustic Source," U.S. Patent 7,260,023, Aug. 21, 2007.

Analysis of the Elasticity of Fibrous Brain Structures Using Sound

A.J. Romano and B.H. Houston
Acoustics Division

Introduction: The noninvasive evaluation of the elastic properties of the human brain is a very active area of research. This is a promising method of analysis in the sense that if the material properties of the brain can be determined with accuracy, they may provide a valuable metric for the evaluation of its state of health including conditions such as traumatic brain injury (TBI), Alzheimer’s disease, multiple sclerosis (MS), and amyotrophic lateral sclerosis (ALS). It has been demonstrated that sound can be used to noninvasively interrogate biological tissues, since the wavelengths of the sound waves in the tissues are directly related to local elastic stiffness values.¹ This method has previously been applied to the brain; however, efforts to date tend to homogenize the brain structures to provide “effective” stiffness and viscoelastic parameters. Here we apply a method that attempts to track waves traveling along white matter pathways such as the cortico-spinal tract (CSTs) and the corpus callosum. These structures

differ from grey matter in that they are comprised of fiber bundles, and can act as waveguides for sound propagation.

Two recent technological breakthroughs enabled the creation of our approach. The first was the development of diffusion tensor imaging (DTI),² which provides a mapping of the pathways of fibrous structures based on water diffusion. The second was the development of magnetic resonance elastography (MRE),¹ which provides a measurement of sound waves throughout biological media. Using the fusion of these two measurement methods, we developed an approach called waveguide-constrained MRE^{3,4} to investigate the elasticity of fibrous structures. Here, we apply this method to the CSTs of five healthy human volunteers.

Methods: Waveguide-constrained MRE requires a knowledge of the pathways along which elastic waves may travel and a measurement of the dynamic displacements within the volume surrounding the pathways. Given a knowledge of the position vectors of the pathways, a spatial-spectral filter, in the form of a spatially dependent Radon transform, is applied to the measured displacements in an attempt to identify only those waves that are traveling parallel along the fiber at

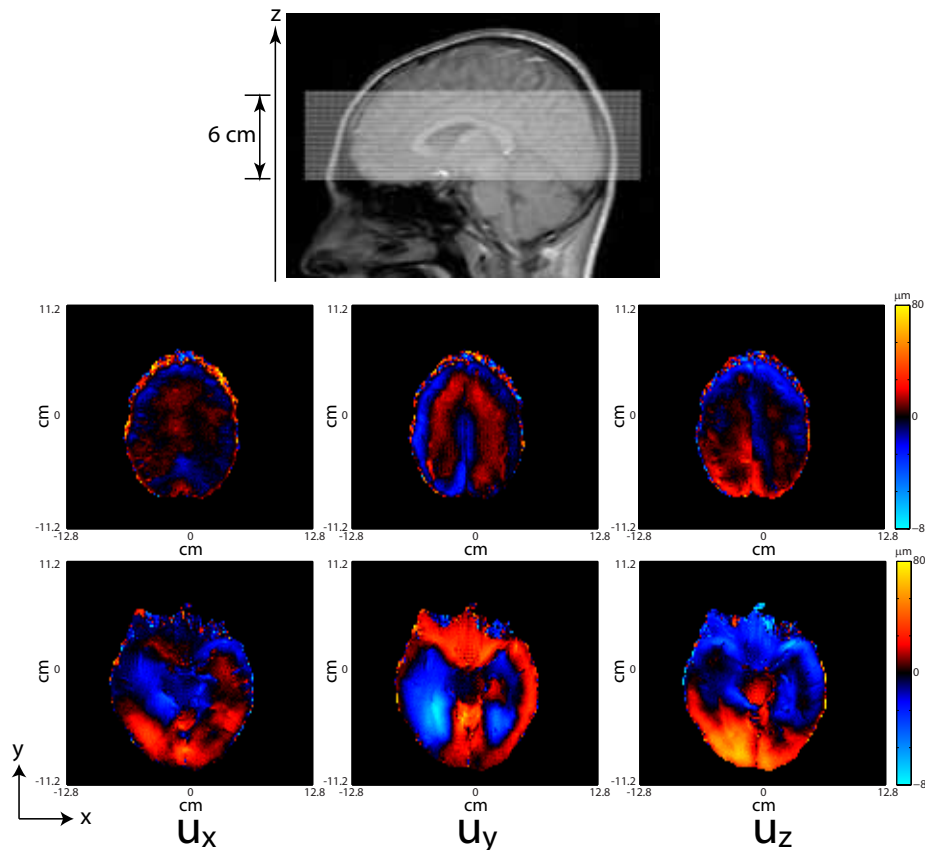


FIGURE 3 MRI of the head and X,Y, and Z displacements at the top and bottom of the field of view.

every point as if it were a zero-order waveguide mode. Further, a Helmholtz decomposition is performed, which separates the total field into its longitudinal and transverse components. Finally, anisotropic inversions are then applied to these filtered displacements, yielding local stiffness values.

For the MRE measurement, the experiment was made using a standard 1.5T clinical MRI scanner (Siemens, Erlangen, Germany). A head-cradle extended-piston driver was used for 50 Hz harmonic head stimulation. A single-shot spin-echo echo planar imaging (EPI) sequence was used for acquiring three Cartesian components of the wave field in 30 adjacent transversal slices with a $2 \times 2 \times 2 \text{ mm}^3$ isotropic image resolution and eight time steps over the vibration period.

For the fiber position measurement, DTI data was acquired using a single-shot EPI sequence with 12 non-colinear directions. Tensor calculation and tractography along the CST was performed using the tools from the FMRIB Software Library (FSL).

Results: Figure 3 shows the MRI of the head as well as the positions of the X, Y, and Z displacement components on the top and bottom of the field of view. Figure 4 shows the results from DTI for an evaluation of the fiber pathways that comprise the CST of a single volunteer, as well as the results of applying the

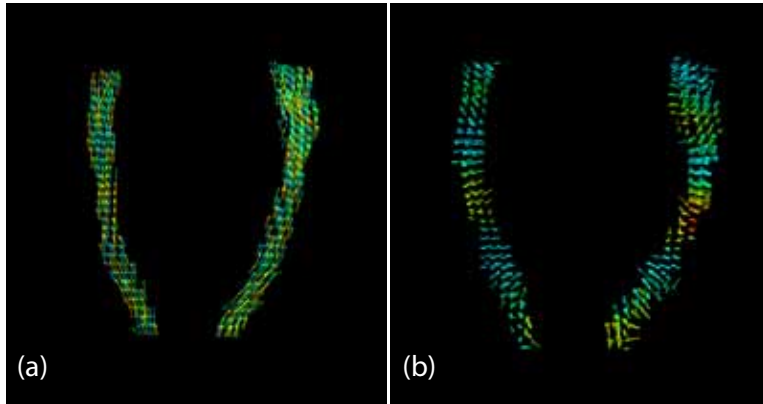


FIGURE 4
a) DTI showing the pathways, and b) the corresponding filtered shear waves along the CST.

spatial-spectral filter to the MRE data along the CST fibers. Figure 5 shows the results of the application of the anisotropic inversion for an evaluation of the local shear stiffness value, C_{44} , within the fiber's local reference frame for all five volunteers. While estimates for brain shear stiffness vary considerably in the literature, average values of around 2 kPa have been reported for the mean shear modulus within slices of healthy samples that include both grey and white matter. Here, the shear stiffness values along the white matter tracts appear to vary from around 2 to 4 kPa (i.e., shear wave

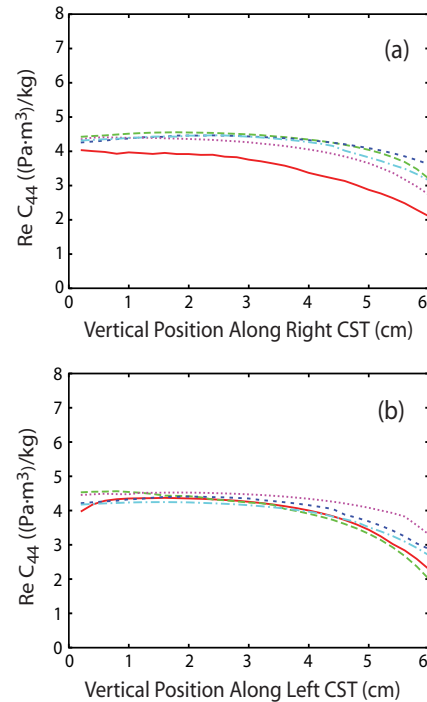


FIGURE 5
Stiffness values for elastic coefficients C_{44} within the right (a) and left (b) CSTs for all five volunteers.

velocities vary from 2.1 to 2.4 m/s) and are spatially dependent as we follow along the right and left CSTs from the bottom to the top of the head, while the compressional waves along the fibers have a much higher wave velocity ($\sim 5 \text{ m/s}$). Future research will apply this approach to other brain structures and different frequencies.

Acknowledgments: This work was supported by the Office of Naval Research. Thanks to Dr. Ingolf Sack and Dr. Michael Scheel of the Department of Radiology, Charité-Universitätsmedizin, Berlin, Germany, for providing all measurements used in this work.

[Sponsored by ONR]

References

- ¹R. Muthupillai, D.J. Lomas, P.J. Rossman, J.F. Greenleaf, A. Manduca, and R.L. Ehman, "Magnetic Resonance Elastography by Direct Visualization of Propagating Acoustic Strain Waves," *Science* **269**, 1854–1857 (1995).
- ²P.J. Basser, J. Mattiello, and D. Le Bihan, "MR Diffusion Tensor Spectroscopy and Imaging," *Biophysical Journal* **66**, 259–267 (1994).
- ³A.J. Romano, P.B. Abraham, P.J. Rossman, J.A. Bucaro, and R.L. Ehman, "Determination and Analysis of Guided Wave Propagation Using Magnetic Resonance Elastography," *Magnetic Resonance in Medicine* **54**, 893–900 (2005).

⁴A.J. Romano, M. Scheel, S. Hirsch, J. Braun, and I. Sack, "Investigation of the Anisotropic Properties of White Matter Tracts in the Human Brain Using Waveguide Constrained MR Elastography," 19th Annual Meeting of the International Society for Magnetic Resonance in Medicine, May 2011, Montreal, Canada, poster P1480.

Acoustic Array Performance and Ship Radiated Noise Source Level Estimation in Shallow Waters

S.L. Means, J.S. Rogers, and S.C. Wales
Acoustics Division

Introduction: The Navy's acoustic surveillance and antisubmarine warfare (ASW) mission success depends on the performance of its acoustic signal receiving arrays. The array performance is determined by aperture size, the background acoustic noise field generated by surface vessels, and the complexity of the shallow water acoustic propagation channel. Large arrays provide narrow beams that allow sonar operators to listen between ships (noise windows) and search for submarines. Simulations of array performance used during Naval surveillance and ASW mission training as well as operational planning require the realistic representation of surface vessel radiated acoustic noise fields.

We describe measured acoustic array performance, the temporal variability of surface vessel radiated acoustic noise fields, and an approach to estimate the source level of ship-radiated noise in shallow water.

Experiment: In 2007, the Office of Naval Research deployed a large-aperture (917 m) linear hydrophone array to collect acoustic data off the coast of Fort Lauderdale, Florida, nominally 12 km offshore, in 263 m of water. The experiment sought to measure the array's performance in shallow water environments in the presence of commercial and recreational vessels. Marine-band radar and Automatic Identification System (AIS) data were collected concurrently to track shipping near the array. Figure 6 illustrates the location of the array and the karst bathymetry of the Miami Terrace. The data analyzed here were collected in late summer (August and September).

Median Beam Noise and Noise Window Statistics: Array performance in terms of median beam noise (MBN) and noise window statistics as a function of bearing, frequency, and aperture is obtained through data analysis. The data are split into categories — weekday day (WDD; 312 hours), weekday night (WDN; 282 h), weekend day (WED; 136 h), and weekend night

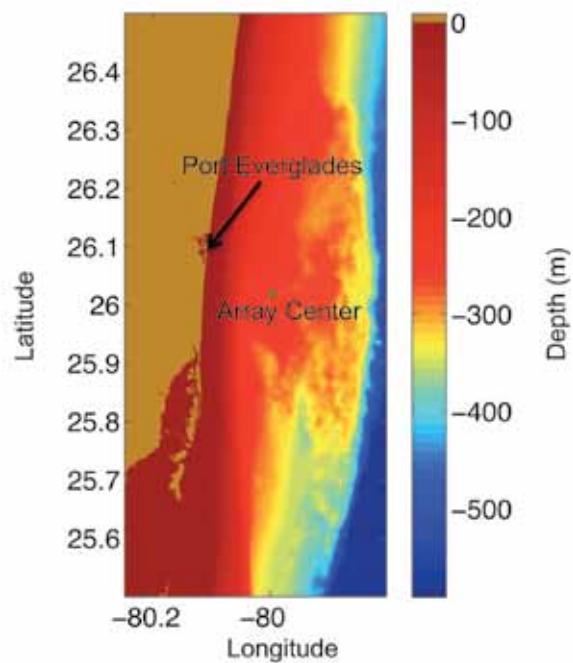


FIGURE 6

Experimental site approximately 12 km off the coast of south Florida. The region east of the array has a karst bottom composed of limestone outcrops and sand pools.

(WEN; 136 h) — so that temporal variations in shipping, both commercial and recreational, might be observed. Figure 7(a) (top row) shows the MBN received on the quarter, half, and full apertures for the four time categories at 416 Hz, near the upper limit of the array. It is noticed, in general, that the noise levels increase from WEN to WDN to WDD to WED. In particular, the WED seaward-bearing noise levels are elevated above the WDD by ~3 dB. This is due to the many recreational vessels distributed over the entire region rather than in commercial shipping lanes. Although not shown here, the levels are more elevated at this frequency (416 Hz) than observed at lower frequencies. This fits known characteristics of recreational and commercial vessels; recreational vessels radiate proportionally more acoustic energy at higher frequencies relative to large, commercial vessels.

Noise windows are time periods in which an array may observe "quiet" regions in between passing ships. These windows provide opportunity of enhanced surveillance of low-noise submarines. For this study, a noise window is defined as a time period in which the background noise level drops 3 dB below the MBN. Figure 7(b) illustrates the probability, rate, and duration of the occurrence of noise windows during WDDs on the three apertures at 416 Hz. One sees that the noise window occurrences are strongly dependent on bearing due to shipping traffic through Port Everglades; the high-noise bearings of the MBN manifest as lower probabilities and higher rates of noise windows. As

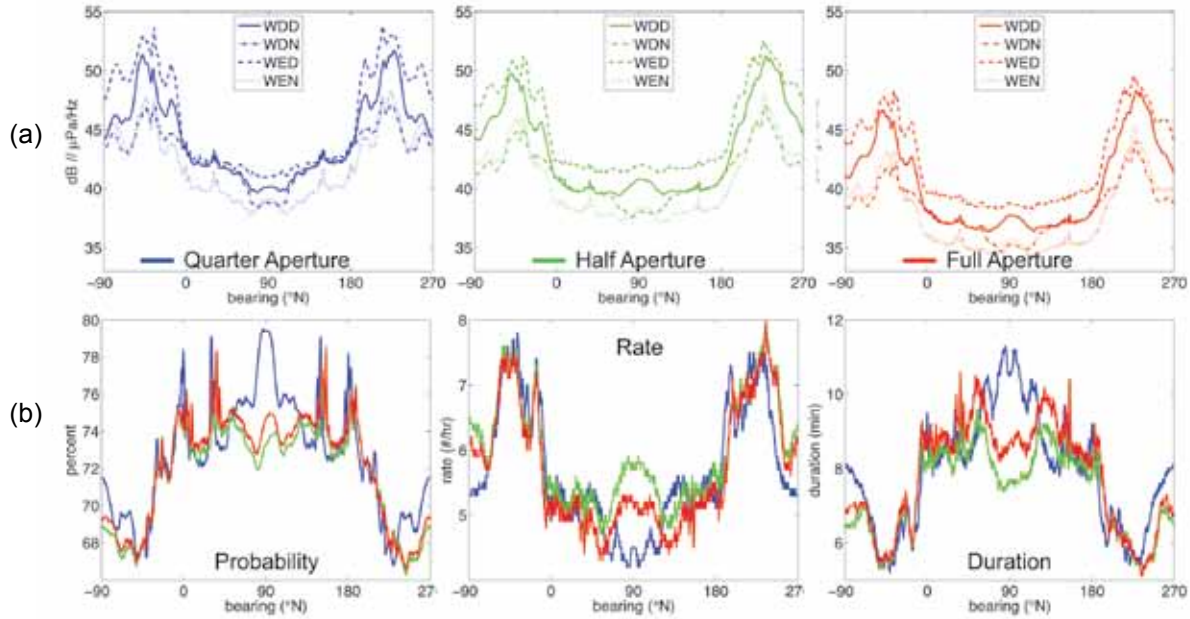


FIGURE 7 (a) Median beam noise for three apertures and four time period classifications at 416 Hz. (b) Noise window statistics (probability, rate, and duration) of WDD noise for quarter, half, and full apertures at 416 Hz.

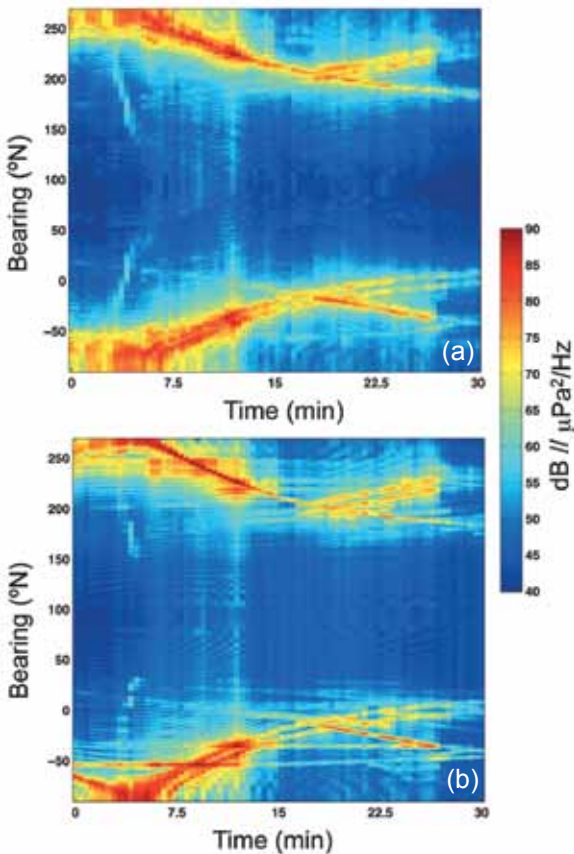


FIGURE 8 (a) Conventional BTR taken from a 30-minute segment of array data. (b) Reconstructed BTR obtained after SL estimation.

expected, the rate and duration of occurrence are inversely proportional to each other. Through such analysis, one may optimally design an array and detection algorithms for surveillance in a given environment.

Ambient Noise Modeling: The ability to accurately estimate shipping source levels (SLs) from the acoustic noise data is an essential step toward creating a forecast model of the ambient noise field. Individual ship SL estimates are computed by solving the system of linear equations, governed by the sonar equation, that relate source level to transmission loss (TL) and beamformer response. Here, beamformer response is known and transmission loss can be modeled from ship positions determined from AIS reports and local radar data. Since source levels must be positive, they are solved for with a non-negative least squares algorithm. Figure 8(a) shows a conventional beamformed bearing-time record (BTR) taken from a 30-minute segment of array data at 104 Hz. SLs are estimated from the beamformed data in Fig. 8(a), then reconstructed using the computed TL and beamformer response to form the BTR shown in Fig. 8(b). A side-by-side comparison shows 3.5 dB mean squared error between the two surfaces. A suitable model of the karst bottom (see Fig. 6) developed for this project was necessary to compute TLs of sufficient detail to achieve this level of mean squared error.

Summary: The acoustic data obtained on a very large horizontal array over extended time periods along with comprehensive measurements of shipping posi-

tions allowed us to study the performance parameters of large-aperture arrays and develop techniques for ship source level estimation. The understanding of acoustic array performance and the ability to estimate ship-radiated acoustic noise source levels in complex shallow water environments with heavy shipping will serve to improve the reliability of Naval acoustic surveillance and ASW operations training and planning.

[Sponsored by the NRL Base Program (CNR funded)]



Nonlinear Poroacoustics: From Kinks to Shocks

P.M. Jordan¹ and J.K. Fulford²

¹Acoustics Division

²Acoustics Division (retired)

Nonlinear Poroacoustics: The study of sound propagating in fluid-saturated porous media, often referred to as poroacoustics, is an important subfield of acoustics, and one which has recently experienced a renewal of interest among researchers (see, for example, Ref. 1 and those therein). If the signal strengths involved are relatively weak and the propagation distances of interest are relatively short, then, just as under

classical acoustics theory, the mathematical models that describe poroacoustic waves involve only linear partial differential equations. If, on the other hand, these conditions are not satisfied, then models based on the linear theory of sound propagation must be set aside, as nonlinear effects, being cumulative over distance traveled, must be taken into account. However, while nonlinear poroacoustic theories are able to capture the salient physics that underlies this class of compressible flow, the mathematical challenges posed by these theories, and by extension the nonlinear model equations derived from them, often dissuade researchers from attempts aimed at finding analytical solutions.

Kinks, Acceleration Waves, and Shocks: Recently, we have succeeded in obtaining what is, possibly, the first exact solution to the set of fully nonlinear, one-dimensional equations governing acoustic propagation in a gas that permeates a class of rigid porous media.² Employing primarily the methods and tools of classical mathematical analysis, we not only uncovered a host of new analytical results, but our investigation also predicts the existence of unexpected, and possibly exploitable, nonlinear (physical) phenomena associated with this case of poroacoustic flow. The following are four of the major findings reported in Ref. 2: (i) established the existence of three distinct propagation regimes (see Fig. 9), specifically, kink, acceleration wave, and shock,

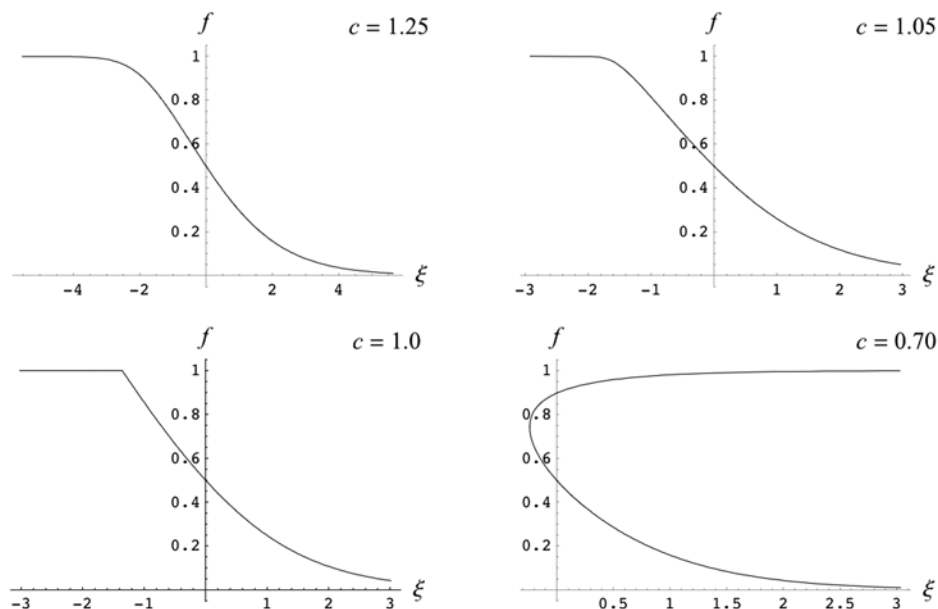


FIGURE 9

As the value of c is decreased from greater than to less than unity, we observe the transition from smooth, but increasing asymmetric, kink-type waveforms, for $c = 1.25$ to $c = 1.05$, to one that admits a corner, and thus an acceleration wave, for $c = 1.0$, to finally a dual-valued solution profile, which in this case signals the presence of a shock, for $c = 0.70$. Here, $\gamma = 7/5$, corresponding to a diatomic gas, $\kappa = 1$, and $f_w = 0.5$; see Ref. 2 for the definitions of f , ξ , and the parameters mentioned above.

which correspond to $c > 1$, $c = 1$, and $c < 1$, respectively, where the positive constant c denotes the speed of the traveling waveform; (ii) confirmed the finding reported in Ref. 3 of a critical amplitude value associated with poroacoustic acceleration waves, namely, the constant α^* , which represents the ratio of attenuation (as described by Darcy's law) to nonlinearity; (iii) derived explicit expressions for the amplitudes of the shock and acceleration waves that occur for $c \leq 1$, respectively; and (iv), uncovered the surprising appearance of the famous number ϕ , known as the *Golden Ratio*, in the solution corresponding to the case of a diatomic gas, an example of which is air.

[Sponsored by the NRL Base Program (CNR funded)]

References

- ¹ B. Straughan, *Stability and Wave Motion in Porous Media* (Springer, New York, 2008).
- ² P.M. Jordan and J.K. Fulford, "A Note on Poroacoustic Traveling Waves Under Darcy's Law: Exact Solutions," *Applications of Mathematics* **56**, 99–115 (2011).
- ³ P.M. Jordan, "Growth and Decay of Acoustic Acceleration Waves in Darcy-type Porous Media," *Proc. of the Royal Society A* **461**, 2749–2766 (2005).

